

## Effect of Short Heat Treatment of Amorphous Metal Alloy on Decolorization Dye Mendola Blue

Khrystyna Khrushchyk<sup>1,2</sup>, Katarzyna Balin<sup>2</sup>, Vasyl Kordan<sup>1</sup>,  
Sylwia Golba<sup>2</sup>, Malgorzata Karolus<sup>2</sup>, Lidiya Boichyshyn<sup>1</sup>

<sup>1</sup> Ivan Franko National University of Lviv, Universytetska St. 1, Lviv, 79000, Ukraine

<sup>2</sup> University of Silesia in Katowice, Bankowa 12, 40-007 Katowice, Poland

\* Corresponding author's e-mail: khrystyna.khrushchyk@us.edu.pl

### ABSTRACT

It was established that the change in the structure of the amorphous metal alloy (AMA) as a result of heat treatment of the amorphous metal alloy  $Al_{87}Gd_5Ni_4Fe_4$  at  $T = 645 \pm 1$  K significantly affects the decolorization of the dye Basic Blue 6/Mendola Blue (BB6/MB) at  $pH = 1.7 \pm 0.3$ . The MB solution with a concentration of  $4.39 \mu M$  was decolorized by 99% within 27 hours, in the case of annealed AMAs for 30, 45, 60 min., which is 3.8 times more effective than in the case of as-cast AMAs. A change in the AMA structure due to annealing was established by X-ray analysis; kinetic analysis was performed based on experimental data and the kinetic parameters (kobs,  $t_{1/2}$ ,  $k_{sa}$ , etc.) of the MB decolorization reaction were calculated. The surface of AMAs after reaction with aniline dye MB and the proposed scheme of decolorization of aniline dye MB using AMAs  $Al_{87}Gd_5Ni_4Fe_4$  were suggested.

**Keywords:** amorphous metal alloy, decolorization, UV-visible spectrophotometry, Basic Blue 6/Mendola Blue, wastewater treatment.

### INTRODUCTION

With the rapid development of modern industry, different types of wastewater discharge pose a serious threat to ecological diversity due to their adverse effects [1]. Approximately 70–75% of all the dyes used in industry are azo dyes [2, 3]. For example, dye-containing wastewater is generated in printing, dyeing, textile and plastics industries [4]. Azo dyes and aniline dyes belong to the largest class of synthetic dyes by a great variety of structure and color [2]. After using dyes in the dyeing process, 10–15% of them end up in the sewage [5]. The authors [4, 6, 7] describes the negative impact of synthetic dyes on the human body (e.g. negative impacts of textile dyes on human health from dermatitis to central nervous system, digestive system, renal system, ect.) and flora and fauna in general. Therefore, it is important to use a fast, inexpensive and reliable way of decomposing dyes in waste. Dye treatment methods can be divided into several types [8, 9]: physical

and chemical methods (adsorption method [10], coagulation, filtration, ion exchange, ultrasonic method, high-energy physical method), chemical treatment methods (ozonation, hypochlorite ion, oxidation method), electrochemical methods (electrochemical oxidation, indirect electro-oxidation with strong oxidants, photoassisted electrochemical methods, electrocoagulation [11, 12], electrochemical reduction), advanced oxidation processes (AOPs) [13–15], microbiological treatments (pure cultures, mixed cultures), and enzymatic decomposition. The authors [16] summarizes the main technologies utilized for the removal of pollutants. Several years ago, it was discovered that amorphous metal alloys based on magnesium [17], iron [18–26], aluminium [26, 27] able to discolour and destroy dyes of different structures. In general basic dyes are cationic compounds that are used for dyeing acid-group containing fibers, usually synthetic fibers like modified polyacryl. They bind to the acid groups of the fibers. Most basic dyes are diarylmethane,

triarylmethane, anthraquinone or azo compounds [28, 29]. The authors of the article [17] shown that solutions of Direct Blue 2B (DB2B) and Acid Orange II with a concentration of 100 mg/l can be almost completely decoloured by the tapes of amorphous metal alloy  $Mg_{63}Cu_{16.8}Ag_{11.2}Er_9$  within 30 min. The analysis based on experimental data showed that the decolouration of azo dye solutions occurred due to physical adsorption. The authors of [29] found that the most effective discoloration of DB2B solution with amorphous metal alloys based on aluminium  $Al_{91-x}Ni_9Y_x$  ( $x = 0, 3, 6, 9\%$ ) occurs at pH = 2. For pH = 2, due to the refreshing effect of  $H^+$ , the azo dye solution can be continuously degraded by metallic glass. For pH = 7, the reaction is carried out in two stages: in the first stage, the reaction rate is rather slow,  $t_0 = 5$  days. In the second stage,  $t_0 = 2$  h. The found that the fastest discoloration reaction of the dye occurs in an acidic environment.

It is known that aluminium-based AMAs doped with transition and rare earth elements improve their mechanical properties [30, 31], as a result of thermal modification, so the aim of this work is to determine the effect of thermal modification of aluminium-based AMAs  $Al_{87}Gd_5Ni_4Fe_4$  on the decolouration rate of MB dye.

## MATERIALS AND METHODS

Amorphous metal ribbons based on aluminium with a thickness of 35  $\mu m$  were received at the Kurdyumov Institute for Metal Physics of the Ukrainian National Academy of Sciences (Kyiv). The curves of differential scanning calorimetry of the initial amorphous alloys based on aluminium were constructed in the Institute of Materials Science of the University of Silesia in Katowice with the help of a Perkin–Elmer Pyris-1 calorimeter for the rates of heating of the samples equal to 10 K/min. The temperature of heat treatment of AMAs were determined from DSC-curves. The X-ray diffraction analysis was performed by using the PANalytical Empyrean Diffractometer with Cu-K $\alpha$  radiation ( $\lambda K\alpha_1 = 1.5418 \text{ \AA}$ ) and the PIX-cell detector. Phase analysis was done basing on the HighScore Plus PANalytical software integrated with the ICDD PDF4 + 2018 crystallographic database. For all the analyzed alloys, using the Rietveld analysis [32, 33] and the Williamson–Hall theory [34], the unit cell parameters of the main identified nano- and microstructural phases

were determined, the size of crystallites and lattice strains were determined as well [35, 36]. The change of morphology of AMA was observed by scanning electron microscope (Tescan VEGA 3 LMU) and an energy dispersive (EDS) X-ray microanalyser (Oxford Instruments Aztec ONE with X-MaxN20 detector). The chemical composition of AMAs samples was analyzed using X-ray photoelectron spectroscopy. The X-ray Photoelectron Spectroscopy measurements were taken using a Physical Electronic XPS spectrometer (Physical Electronics PHI 5700, Chanhassen, MN, U.S.A.). A monochromatic radiation from the Al K $\alpha$  anode (1486.6 eV) was applied. The measurements were taken from the as-prepared surfaces at room temperature. The analysis area from which photoelectrons were collected was selected using a diaphragm and was of the size of 80  $\mu m$  in diameter. The XPS measurements were carried out for the survey scan, core levels detected elements. All measurements were executed at a 45° angle with a pass energy of 187.85 eV, step – 0.8 eV and 23.50 eV, step – 0.05 eV for survey and high-resolution spectra, respectively. Atomic calculations and fitting processes were performed using MULTIPAK (v.9.6.0.1, ULVAC PHI, Chigasaki, Japan) software from Physical Electronics. Due to the observed charging of the sample surface, obtained XPS spectra were calibrated using the C1s peak (B.E. = 284.6 eV). The deconvolution of the core level lines was performed by applying the Shirley-type background and the generally Gaussian–Lorentzian shape of lines. Quantum-chemical calculations for MB were carried out by means of the semiempirical program MOPAC2016 [37] with the graphical interface Winmstar [38]. We used semiempirical method PM7  $\pm$  taking into account the dielectric constant of water ( $\epsilon = 78.4$ ) as a solvent to optimize the geometric structure and calculate the heat of formation ( $\Delta fH^{298}$ ), energies of the highest occupied (HOMO) and lowest unoccupied (LUMO) molecular orbitals, as well as charges on atoms by Mulliken. The degradation of the MB dye was monitored by ultraviolet-visible absorption spectrophotometer (WPA Bioware II).

## RESULTS AND DISCUSSION

The kinetic of destruction of aniline dye ( $C_{18}H_{15}ClN_2O$  hereafter named Mendola Blue) were carried out in aqueous solutions with

concentrations of 4.39  $\mu\text{M}$  was prepared by dissolving the azo dye powders (Fig. 1b) with deionized water and  $\text{pH} = 1.7 \pm 0.3$  (the pH was adjusted with 1M HCl (Fig. 2b)). The working area of each AMAs equal to  $1\text{cm}^2$  with a size of  $10 \times 5 \times 0.035$  mm with a specific surface area of about  $0.0058(1) \text{ m}^2/\text{g}$ . The solution was not stirred during degradation. 2 mL solution was extracted each time for ultraviolet-visible absorption spectrophotometer (WPA Bioware II) test to measure the concentration decay of solutions (Fig. 1a).

From Figure 1a shows that due to the degradation of the MB dye, the peak (635 nm) shifts by 5–8 nm towards lower values, indicating the possibility of complex formation in the studied MB solution [39].

The phase transition temperatures for AMAs were determined from DSC-curves (Fig. 2a). In this work for annealing of AMAs were used  $T_3 = 645 \pm 1$  K (temperature of stable crystallization) for second peak of AMAs  $\text{Al}_{87}\text{Gd}_5\text{Ni}_4\text{Fe}_4$ . The rate

of heating the furnace to the selected temperature was about 17–20 K/min.

One can see that after 5 minutes of annealing, a nanostructure is formed in the alloys, which after another 15 minutes leads to the formation of a microcrystalline structure. Basing on the ICDD PDF4+ data base, the phase analysis was done. The solid solution  $\text{Al}(X)$  and  $\text{GdFe}_2$  and  $\text{GdNiAl}_3$  phases were identified in studied alloys. Detailed results, together with the determined lattice parameters, crystallite sizes and lattice strains, are presented in Table 1.

The decoloration kinetics of the MB dye was studied for the original, thermally modified AMAs at solution temperatures of 18, 30, 40 and 50  $^\circ\text{C}$ . The relevant expressions are as follows [17, 40]:

$$C_t/C_0 = \exp(-k_{obs} \cdot t) \quad (1)$$

where:  $k_{obs}$  ( $\text{h}^{-1}$ ) – is the observed rate constant,  $t$  – is the reaction time,  $C_0$  – is the initial concentration of the MB solution,  $C_t$  – is the concentration of MB remaining in the solution at the reaction time of  $t$ .

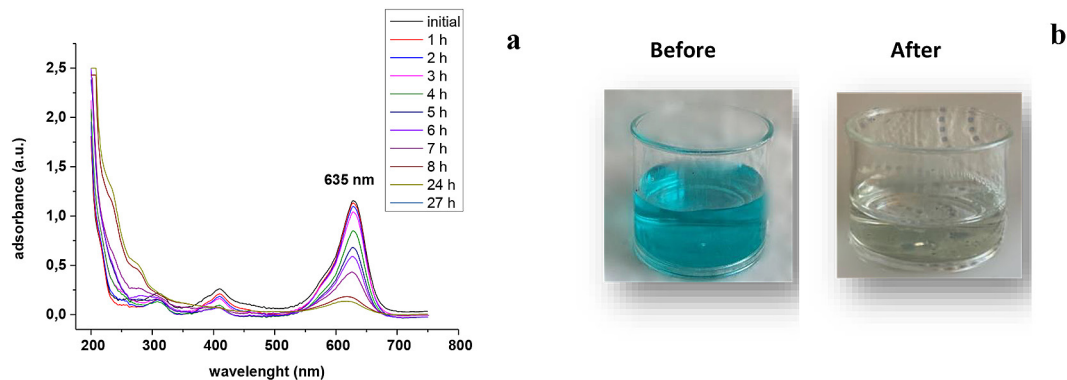


**Figure 1.** (a) UV– spectrum of Mendola Blue solution ( $C_M = 4.39 \mu\text{M}$ ) at  $\text{pH} = 1.7 \pm 0.3$  at room temperature; (b) Changes in the color of MB after the decolorization reaction using AMAs during 27 hours

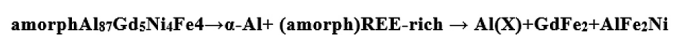
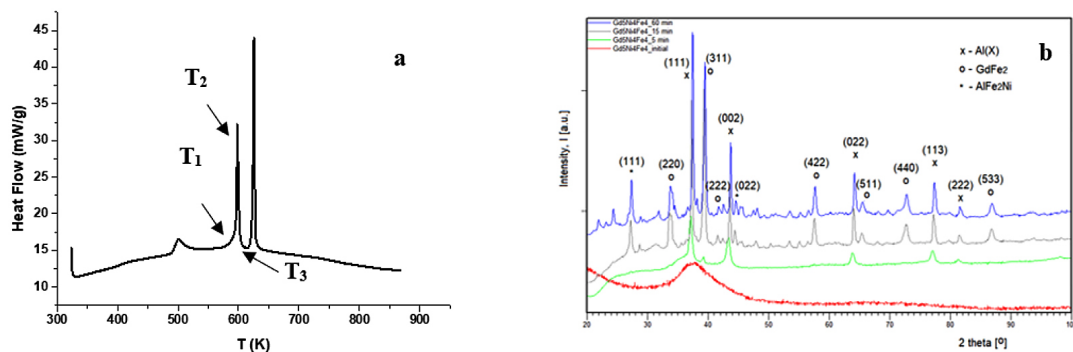


**Figure 2.** (a) DSC-curves ( $\beta = 20$  K/min) of amorphous alloys of the  $\text{Al}_{87}\text{Gd}_5\text{Ni}_4\text{Fe}_4$  in the temperature range of 300–900 K; (b) The X-ray diffraction patterns of AMA amorphous alloys with the composition of  $\text{Al}_{87}\text{Gd}_5\text{Ni}_4\text{Fe}_4$  in initial state and after annealing of 5, 15, 30, 45, 60 min

**Table 1.** The unit cell parameters, size of crystallites and lattice strains obtained for the nano- and microstructural main phases identified in tested AMA alloys

Theoretical data: ICDD PDF4+ card number Space group Lattice parameters		Al(X), where X=Gd,Ni,Fe	GdFe <sub>2</sub>	GdNiAl <sub>3</sub>
		01-089-2837 Fm-3m, cubic a = 4.0592 Å	04-004-0708 Fd-3m, cubic a = 7.3940 Å	04-018-2016 Pnma, orthorhombic a = 8.1640 Å b = 4.0680 Å c = 10.6660 Å
Al <sub>87</sub> Gd <sub>5</sub> Ni <sub>4</sub> Fe <sub>4</sub>	5 min	a = 4.0764(9) Å D = 125 Å h = 0.25 %	a = 7.3967(3) Å D = 100 Å h = 0.36 %	–
	15 min/ 60 min.	a = 4.0732(1) Å D = 270 Å h = 0.12 %	a = 7.4967(9) Å D = 220 Å h = 0.15 %	a = 7.7966(2) Å b = 3.799(9) Å c = 10.1384(2) Å D = 220 Å; h = 0.15 %

It was found by nonlinear curve fitting that the residual rate of MB concentration changed with time according to the first order reaction model in chemical reaction kinetics.

$$t_{1/2} = \ln 2/k \quad (2)$$

where:  $k$  – is the reaction rate constant,  $t$  – is the reaction time,  $t_{1/2}$  – is half-period.

Dye decolorization ( $D\%$ ) efficiency MB was determined as follows [41, 42]:

$$D\% = 100 - \left( \frac{\text{initial abs.} - \text{observed abs.}}{\text{initial abs.}} \right) \cdot 100 \quad (3)$$

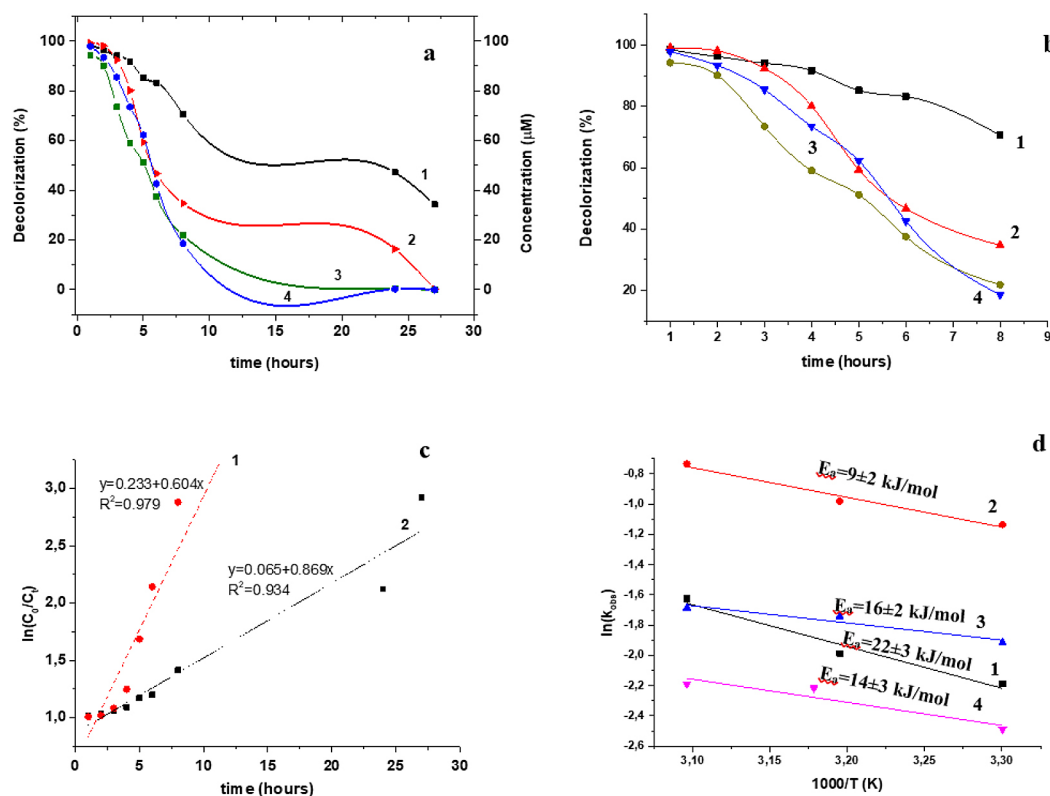
The relevant kinetic parameters  $k$ ,  $t_{1/2}$ , and degradation rate obtained by fitting Figure 4c and results are shown in Table 2.

Figure 3a and Table 2 show a decrease in the concentration of MB dye in solution, which is 1.75  $\mu\text{M}$  for the initial sample of AMA Al<sub>87</sub>Gd<sub>5</sub>Ni<sub>4</sub>Fe<sub>4</sub> at the  $T = 18^\circ\text{C}$  of the experiment and 0.264–0.04  $\mu\text{M}$  for the heat-treated AMAs. To compare the decolorization rate of the aniline dye MB of the initial and annealed AMAs samples were used a normalized rate constant ( $k_{sa}$ ) [17] defined as  $k_{obs}/(S_{area\ of\ AMA}/V_{dye})$ .  $K_{sa}$  for initial AMA equal to 3.25  $\text{L}\cdot\text{m}^{-2}\text{h}^{-1}$  and 11.65  $\text{L}\cdot\text{m}^{-2}\text{h}^{-1}$ ; 15.35  $\text{L}\cdot\text{m}^{-2}\text{h}^{-1}$ ; 8.00  $\text{L}\cdot\text{m}^{-2}\text{h}^{-1}$  for annealed AMAs for 30, 45, 60 min, respectively.

The reaction rate of MB decolouration using thermally modified AMAs Al<sub>87</sub>Gd<sub>5</sub>Ni<sub>4</sub>Fe<sub>4</sub> samples for 30, 45, 60 min increases the decolouration rate of MB dye during the first eight hours of

**Table 2.** Degradation reaction kinetic parameters

Time of heat treatment of AMA, min	Temperature of solution of BB6, °C	$k_{obs}$ ( $\text{h}^{-1}$ )	$t_{1/2}$ (h)	Degradation (%)
Initial	18 (room temperature)	0.06	10.66	65
	30	0.11	6.30	93
	40	0.13	5.05	99
	50	0.19	3.52	96
Annealed during 30 min	18 (room temperature)	0.23	2.97	99
	30	0.15	4.71	97
	40	0.18	3.96	94
	50	0.19	3.75	99
Annealed during 45 min	18 (room temperature)	0.32	2.16	91
	30	0.32	2.16	91
	40	0.37	1.85	93
	50	0.48	1.44	99
Annealed during 60 min	18 (room temperature)	0.16	4.33	99
	30	0.08	8.35	88
	40	0.11	6.36	93
	50	0.11	6.19	95



**Figure 3.** (a) Dependences of the concentration change on the discoloration reaction time of MB at room temperature for different annealing times of  $\text{Al}_{87}\text{Gd}_5\text{Ni}_4\text{Fe}_4$ : 1-initial, 2–60 min, 3–30 min, 4–45 min. (b) Dependences of the concentration change on the discoloration reaction time of MB for the first eight hours of the experiment at room temperature for different annealing times of  $\text{Al}_{87}\text{Gd}_5\text{Ni}_4\text{Fe}_4$ : 1 – initial, 2 – 60 min, 3 – 30 min, 4 – 45 min. (c) Kinetic curves of  $\ln(C_0/C_t)$  versus discoloration time of MB for different annealing times of  $\text{Al}_{87}\text{Gd}_5\text{Ni}_4\text{Fe}_4$  AMAs: 1 – 45 min, 2 – initial. (d) Kinetic curves of  $\ln(k_{\text{obs}})$  versus  $1000/T$  for different annealing times of  $\text{Al}_{87}\text{Gd}_5\text{Ni}_4\text{Fe}_4$  AMAs: 1 – initial, 2 – 30 min, 3 – 45 min, 4 – 60 min

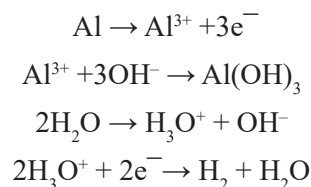
the experiment by 3.8 times (Fig. 4b), and the decoloration efficiency increases from 65% for the original sample to 91-99% for thermally modified samples (Table 2). Increasing the temperature of the MB dye solution to 30, 40, 50 °C increases the decolorisation efficiency when using the initial AMA sample  $\text{Al}_{87}\text{Gd}_5\text{Ni}_4\text{Fe}_4$  to 99%. From Fig. 4a and Table 2 show that the fastest decoloration reaction of the dye at a solution temperature of 18 °C occurs in the presence of a thermally modified AMAs for 45 min. The EDS analysis (Fig. 6, Table 3) shown that the surface of this AMA was depleted in aluminium after the discoloration reaction due to the dissolution and defonding of aluminium ions into the MB dye solution.

During the first eight hours of interaction of AMAs samples with the MB solution, the solution degrades by 80% at an approximate rate of 10% per hour (Fig. 3b). The relatively high activation energy of aluminium dissolution  $22\pm 3$  kJ/mol compared to thermally modified

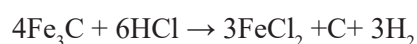
samples indicates that the efficiency decolorization of MB solution.

The SEM images of the AMAs surface  $\text{Al}_{87}\text{Gd}_5\text{Ni}_4\text{Fe}_4$  (contact side) after reaction of decolorization of MB during 27 hours (Fig. 5e 1, 2 and 5h 3) shown ‘pores’ (probable places of aluminium diffusion into the dye solution).

The following reactions probably occur during the interaction of MB with AMA  $\text{Al}_{87}\text{Gd}_5\text{Ni}_4\text{Fe}_4$ :



Using the XPS analysis method (Table 3), it was established that there is 47.54 at.% C1s on the surface of AMA, 17 at. % of which is in the imide form, the following reaction probably also occurs:



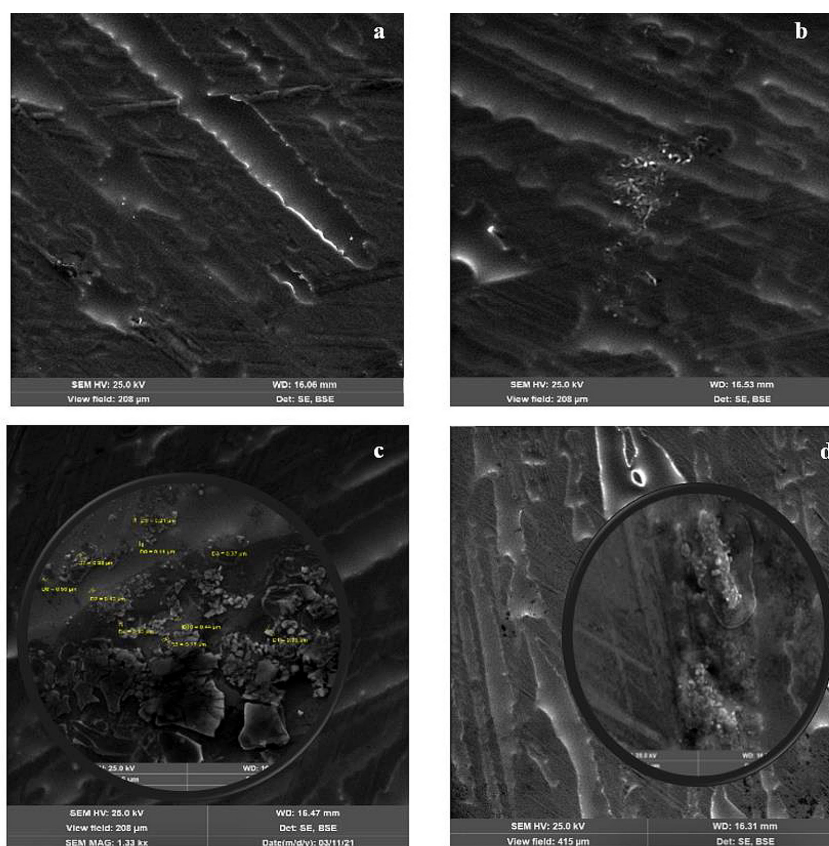


**Figure 4.** SEM images of amorphous surface of  $\text{Al}_{87}\text{Gd}_5\text{Ni}_4\text{Fe}_4$  (contact side): initial (a) and annealed during 30 (b), 45 (c), 60 (d) min. before decolorization of MB dyes

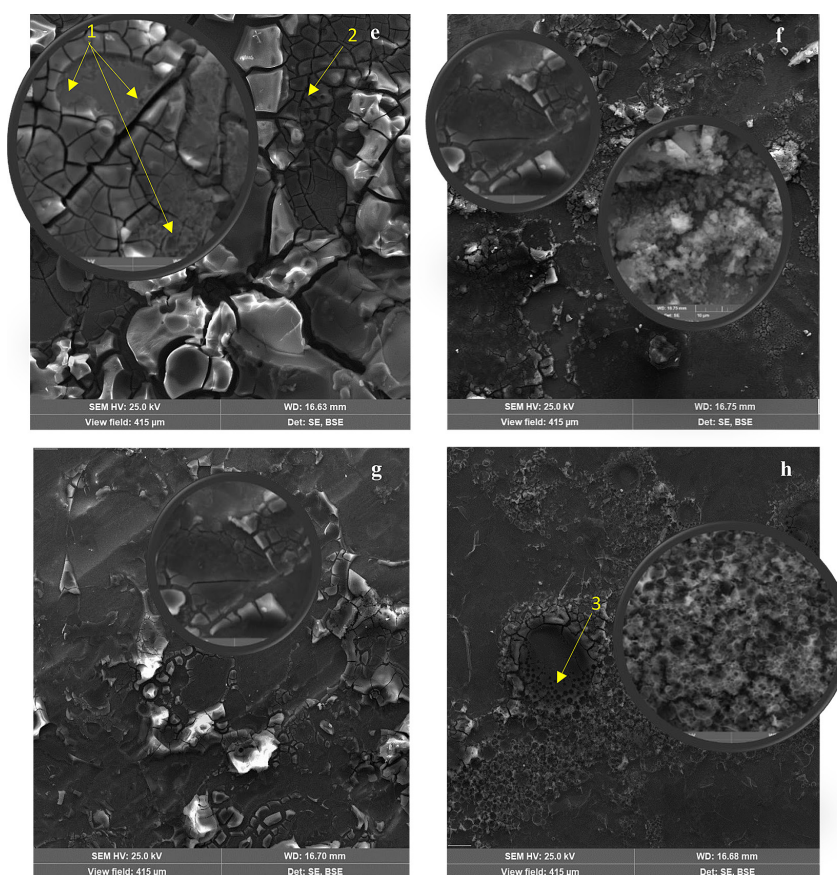


**Figure 5.** SEM images of amorphous surface of  $\text{Al}_{87}\text{Gd}_5\text{Ni}_4\text{Fe}_4$  (contact side) after reaction of decolorization of MB during 27 hours: initial (e) and annealed during 30 (f), 45 (g), 60 (h) min

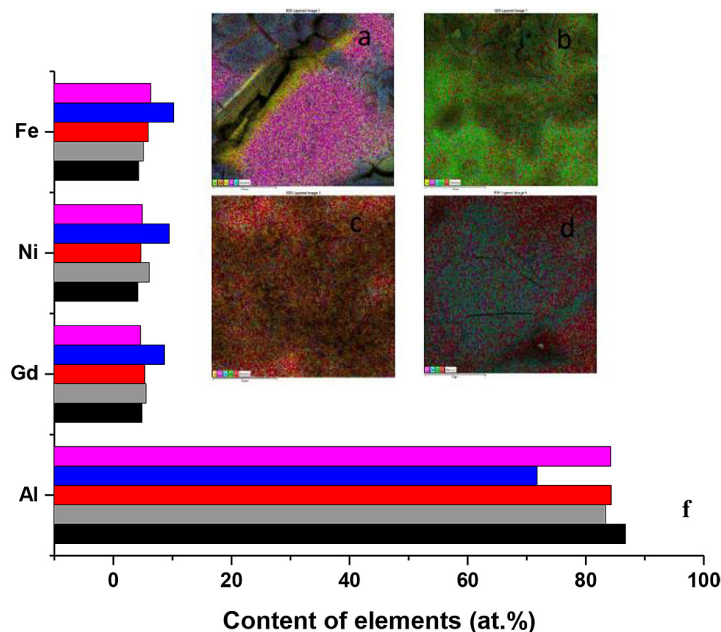


**Figure 6.** EDS images of amorphous surface of  $Al_{87}Gd_5Ni_4Fe_4$  (contact side) after reaction of decolorization of MB during 27 hours: initial (a) and annealed during 30 (b), 45 (c), 60 (d) min. and (f) elements distribution map of amorphous surface of  $Al_{87}Gd_5Ni_4Fe_4$  (contact side) before (black column), after reaction of decolorization of MB during 27 hours: initial (f, grey column) and annealed during 30 min. (f, red column), 45 min. (f, blue column), 60 min. (f, pink column)

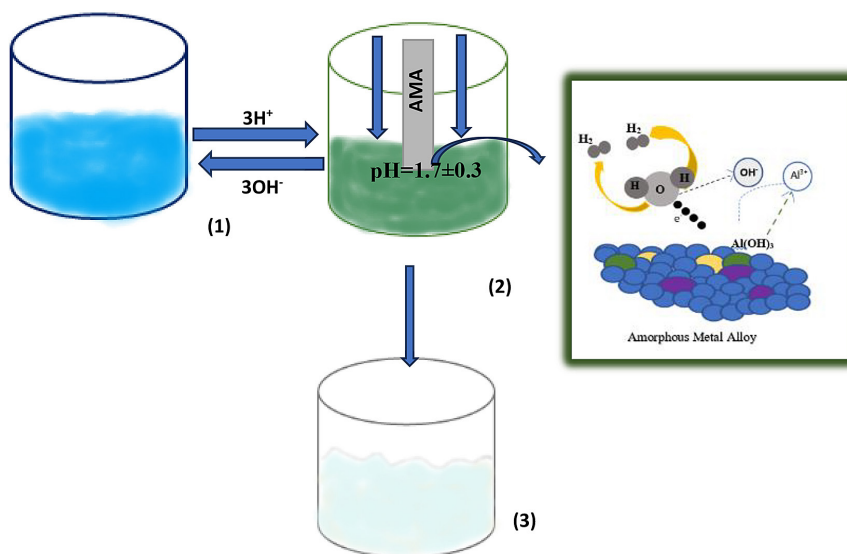


**Figure 7.** A scheme of decolorization of dye Mendola Blue using AMA  $Al_{87}Gd_5Ni_4Fe_4$

**Table 3.** Atomic concentration table

Content of elements (at.%)							
C 1s	N 1s	O 1s	Al 2p	S 2p	Cl 2p	Fe 2p	Gd 3d
47.54	0.39	35.11	12.29	0.84	2.52	1.17	0.15

**Table 4.** The results of calculations of physical-chemical parameters for MB by semi-empirical PM7 quantum-chemical methods

MB	$\Delta_f H^{298}$ , kJ/mol	$I_x$ , eV	HOMO, eV	LUMO, eV	S, Å <sup>2</sup>	V, Å <sup>3</sup>
I	-266.7	7.096	-7.096	-0.987	461.2	674.9
II	-293.7	7.384	-7.384	-0.845	477.7	687.9

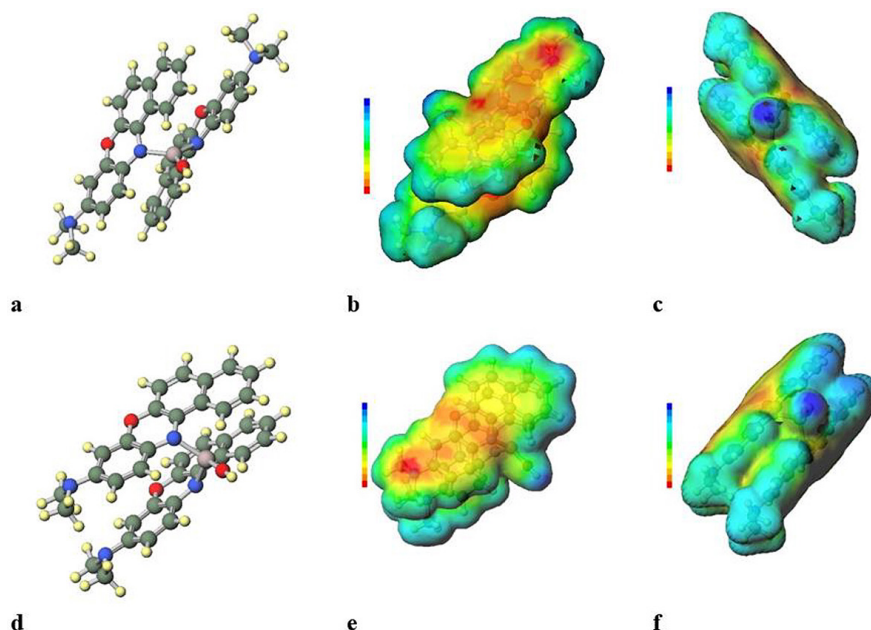


**Figure 8.** The optimal geometrical structure of the conformation of antisymmetric (a, b, c) and symmetric (d, e, f) aluminium complexes with MB: a, d – steric arrangement of atoms in the complexes; b, c, e, f – electron density distribution on the surface of the complexes

The formation of aluminocplexes based on two MB molecules has been modelled. These complexes have two conformational states in which the aminodimethyl groups of the MB molecule are arranged in parallel and antiparallel. The Figure 8 shows the optimal geometrical structures and the distribution of electrostatic potentials on their surface. The conformations of the antisymmetric Figure 8 (a, b, c) and symmetric Figure 8 (d, e, f) complexes of alumina complexes with MB are visualised.

The Table 4 shown the heat of formation of the complex, which takes into account the electronic interaction between the atoms of the complex and the aqueous medium. According to the results shown in the table, the most energetically favourable state is the antisymmetric complex, in which the amino dimethyl groups are located on different sides of the MB molecule forming the complex. The  $\Delta_f H^{298}$  becomes more negative and is  $-293.7$  kJ/mol. The formation of such intermediate complexes probably leads to further destruction of bonds between atoms and discoloration of MB dyes.

## CONCLUSIONS

It was found that the change in the structure of the amorphous metal alloy (AMA) as a result of heat treatment of the amorphous metal alloy

$Al_{87}Gd_5Ni_4Fe_4$  at  $T=645\pm 1$  K significantly affects the decolourisation of the aniline dye Mendola Blue at  $pH = 1.7 \pm 0.3$ . The decolouration efficiency of MB is more than 90% within 27 hours, in the case of annealed AMAs for 30, 45, 60 min, which is 1.5 times more effective than in the case of initial AMA.

The combined effect of AMA annealing and heating of the MB solution leads to a more efficient decolorisation process by a factor of two for the initial  $Al_{87}Gd_5Ni_4Fe_4$  AMA samples and 1.5 times for the annealed sample for 45 min and with a solution temperature of  $45^\circ C$  compared to the annealed sample for 45 min and with a solution temperature of  $18^\circ C$ . Changes in the structure of  $Al_{87}Gd_5Ni_4Fe_4$  AMAs as a result of annealing were found: after 5 minutes of annealing, a nanostructure is formed in the alloys, which after another 15 minutes leads to the formation of a microcrystalline structure.

## REFERENCES

1. Malovanyy M., Palamarchuk O., Trach I., Petruk H., Sakalova H., Soloviy Kh., Vasylynych T., Tymchuk I., Vronska N. 2020. Adsorption extraction of chromium ions (III) with the help of bentonite clays. Journal of Ecological Engineering. 21(7), 178-185. <https://doi.org/10.12911/22998993/125545>

2. Benkhaya S., M'rabet S., Ahmed El. Harfi. 2020. Classifications, properties, recent synthesis and applications of azo dyes. *Heliyon*. 6(1), e03271. 10.1016/j.heliyon.2020.e03271
3. Shah M. 2014. Effective treatment systems for azo dye degradation: a joint venture between physico-chemical and microbiological process international. *Journal of Environmental Bioremediation and Biodegradation*. 2(5), 231-242. 10.12691/ijebb-2-5-4
4. Kochubei V.V., Yaholnyk S.G., Kniaz S.V., Parashchuk L.Y., Malovanyy M.S. 2020. Research into the influence of activation conditions of transcarpathian clinoptilolite on its adsorption capacity. *Pytania khimii i khimicheskoi tekhnologii*. 4, 80-87. doi:10.32434/0321-4095-2020-131-4-80-87
5. Zhang L.C., Jia Z., Lyu F., Liang S.X., Lu J. 2019. A review of catalytic performance of metallic glasses in wastewater treatment: recent progress and prospects. *Progress in Materials Science*. 105, 100576. <https://doi.org/10.1016/j.pmatsci.2019.100576>
6. King-Thom Chun. 2016. Azo dyes and human health: A review. *Journal of Environmental Science and Health*. 34(4), 233-261. <http://dx.doi.org/10.1080/10590501.2016.1236602>
7. Ibrahim Q., Creedon L., Gharbia S. 2022. A literature review of modelling and experimental studies of water treatment by adsorption processes on nanomaterials. *Membranes*. 12(4), 360. <https://doi.org/10.3390/membranes12040360>
8. Naim M.M., El Abd Y.M. 2002. Removal and recovery of dyestuffs from dyeing wastewaters. *Sep. Purif. Methods* 31. 171–228.
9. Dos Santos A.B., Cervantes F.J., van Lier J.B. 2007. Review paper on current technologies for decolourisation of textile wastewaters: perspectives for anaerobic biotechnology. *Bioresour. Technol.* 98. 2369–2385
10. Ramya M., Karthika M., Selvakumar R., et al. 2017. A facile and efficient single step ball milling process for synthesis of partially amorphous Mg-Zn-Ca alloy powders for dye degradation. *Journal Alloy and Compounds*. 695, 185-192. <http://dx.doi.org/10.1016/j.jallcom.2016.11.221>
11. Kochubei V., Yaholnyk S., Bets M., Malovanyy M. 2020. Use of activated clinoptilolite for direct dye-contained wastewater treatment. *Chemistry and Chemical Technology*, 14(3), 386-393. <https://doi.org/10.23939/chcht14.03.386>
12. Daneshvar N., Oladegaragoze A., Djafarzadeh N. 2006. Decolorization of basic dye solutions by electrocoagulation: An investigation of the effect of operational parameters. *Journal of Hazardous Materials*. 129(1-3), 116-122. 10.1016/j.jhazmat.2005.08.033
13. Merzouk B., Madani K., ASekki A. 2010. Using electrocoagulation–electroflotation technology to treat synthetic solution and textile wastewater, two case studies. *Desalination*. 250(2), 573-577. 10.1016/j.desal.2009.09.026
14. Gao J., Qin T., Waclawek S., et al. 2023. The application of advanced oxidation processes (AOPs) to treat unconventional water for fit-for-purpose reuse. *Current Opinion in Chemical Engineering*. 42, 100974. <https://doi.org/10.1016/j.coche.2023.100974>
15. Lopez N., Plaza S., Afkhami A., et al. 2017. Treatment of Diphenhydramine with different AOPs including photo-Fenton at circumneutral pH. *Chemical Engineering Journal*. 318, 112-120. <https://doi.org/10.1016/j.cej.2016.05.127>
16. Kim S.H., Seo J., Hong Y., et al. 2023. Construction of an underwater plasma and Fenton hybrid system for the rapid oxidation of organic dyes and antibiotics. *Journal of Water Process Engineering*. 52, 103519. <https://doi.org/10.1016/j.jwpe.2023.103519>
17. Martínez-Huitle C.A., Brillas E. 2009. Decontamination of wastewaters containing synthetic organic dyes by electrochemical methods: A general review. *Applied Catalysis B: Environmental*, 87(3-4), 105-145. <https://doi.org/10.1016/j.apcatb.2008.09.017>
18. Zhang C., Zhu Z., Zhang H. 2017. Mg-based amorphous alloys for decolorization of azo dyes. *Results in Physics*. 7, 2054-2056. <https://doi.org/10.1016/j.rinp.2017.06.031>
19. Fan J., Guo Y, et al. 2009. Rapid decolorization of azo dye methyl orange in aqueous solution by nanoscale zerovalent iron particles. *Journal of Hazardous Materials*. 166(2-3), 904-910. <https://doi.org/10.1016/j.jhazmat.2008.11.091>
20. Chen J.W., Zheng Z.G., Qiu Z.G., Peng S.Y., et al. 2020. Excellent degradation performance of the Fe<sub>78</sub>Si<sub>11</sub>B<sub>9</sub>P<sub>2</sub> metallic glass in azo dye treatment. *Journal of Physics and Chemistry of Solids*. 145, 109546 <https://doi.org/10.1016/j.jpcs.2020.109546>
21. Wang Q., Yun L., Chen M., Xu D., et al. 2018. Competitive effects of structural heterogeneity and surface chemical states on catalytic efficiency of FeSiBPCu amorphous and nanocrystalline alloys *ACS Applied Nano Materials*. 2, 214-227. 10.1021/acsnm.8b01669
22. Liu P., Zhang J.L., Zha M.Q., Shek C.H. 2014. Synthesis of an Fe rich amorphous structure with a catalytic effect to rapidly decolorize Azo dye at room temperature. *ACS Applied Materials Interfaces*. 6, 5500-5505. <https://doi.org/10.1021/am501014s>
23. Hou L., Wang Q., Fan X. 2019. Effect of Co addition on catalytic activity of FePCCu amorphous alloy for methylene blue degradation. *New Journal of Chemistry*. 43, 6126-6135. <https://doi.org/10.1039/C9NJ00369J>
24. Shi J., Ni B., Zhang J. 2019. Effect of Ni addition on catalytic performance of Fe<sub>87</sub>Si<sub>5</sub>B<sub>2</sub>P<sub>3</sub>Nb<sub>2</sub>Cu<sub>1</sub> amorphous alloys for degrading methylene blue dyes. 9(3), 341 doi:10.3390/met9030341

25. Jia Z., Kang J., Zhang W. 2017. Surface aging behaviour of Fe-based amorphous alloys as catalysts during heterogeneous photo-Fenton-like process for water treatment. *Applied Catalysis B: Environmental*. 204, 537-547. <http://dx.doi.org/10.1016/j.apcatb.2016.12.001>
26. Lonski S., Lukowicz D., Barbusinski K. 2023. Flower-like magnetite nanoparticles with unfunctionalized surface as an efficient catalyst in photo-Fenton degradation of chemical dyes. *Applied Surface Science*. 638, 158127. <https://doi.org/10.1016/j.apsusc.2023.158127>
27. Yang J., Bian X., Bai Y. 2012. Rapid organism degradation function of Fe-based alloys in high concentration wastewater. *Journal of Non-Crystalline Solids*. 358 (18–19), 2571-2574. <https://doi.org/10.1016/j.jnoncrysol.2012.06.002>
28. Chen Q., Ya, Z., Zhang H., Kim K., Wang W. 2021. Role of Nanocrystallites of Al-Based Glasses and H<sub>2</sub>O<sub>2</sub> in Degradation Azo Dyes. *Materials*, 14(1), 39. <https://doi.org/10.3390/ma14010039>
29. Zee, F.P. van der 2002. Anaerobic azo dye reduction. PhD thesis, Wageningen University. pp. 142.
30. Wang P., Wang J.-Q., Li H., Yang H. Fast decolorization of azo dyes in both alkaline and acidic solutions by Al-based metallic glasses. 2017. *Journal of Alloys and Compounds*. 701, 759-767. <http://dx.doi.org/10.1016/j.jallcom.2017.01.168>
31. Herzer G. 2013. Modern soft magnets: Amorphous and nanocrystalline materials. *Acta Materialia*. 61(3), 718-734. <https://doi.org/10.1016/j.actamat.2012.10.040>
32. Boichyshyn L., Khrushchik Kh., Kovbuz M., et al. 2019. Specific features of the transition of amorphous Al<sub>87</sub>REM<sub>5</sub>Ni<sub>8</sub>(Fe) alloys into the crystalline state under the influence of temperature. *Materials Science*. 55(11), 17-26. [10.1007/s11003-019-00246-7](https://doi.org/10.1007/s11003-019-00246-7)
33. Young R.A. 1993. *The Rietveld method*. Oxford University Press.
34. McCusker, L.B.; Von Dreele, R.B.; Cox, D.E.; Louër, D.; Scardi, P. Rietveld refinement guidelines. *J. Appl. Crystallogr.* 1999, 32, 36–50.
35. Williamson G.K., Hall W.H. 1953. X-ray Line Broadening from Filled Aluminium and Wolfram. *Acta Metall*, 1, 22-31.
36. Karolus M. 2006. Applications of Rietveld refinement in Fe–B–Nb alloy structure studies. *Journal of Materials Processing Technology*. 175, 246-250. <https://doi.org/10.1016/j.jmatprotec.2005.04.016>
37. Karolus M., Łągiewka E. 2004. Crystallite size and lattice strain in nanocrystalline Ni-Mo alloys studied by Rietveld refinement. *Journal of Alloys and Compounds*, 367, 235–238. <https://doi.org/10.1016/j.jallcom.2003.08.04>
38. Stewart J.J. Program Package MOPAC2016 (<http://www.openmopac.net>).
39. Senda N. Program Package Winmostar (<http://winmostar.com>).
40. Kovalchuk E.P. 2005. Substance in the interphase. In: Y.P. Kovalchuk, M.M. Yatsyshyn, Y.S. Kovalyshyn (Eds.) *Physical chemistry of thin films*. Ivan Franko National University of Lviv Publishing Centre, pp. 242. (in Ukrainian)
41. Zhang C., Zhu Z., Zhang H., et al. 2012. Rapid decolorization of Acid Orange II aqueous solution by amorphous zero-valent iron. *Journal of Environmental Sciences*. 24(6), 1021-1026. [https://doi.org/10.1016/S1001-0742\(11\)60894-2](https://doi.org/10.1016/S1001-0742(11)60894-2)
42. Fareed A., Zaffar H., Bilal M., Hussain J., Jackson C., Naqvi T.A. 2022. Decolorization of azo dyes by a novel aerobic bacterial strain *Bacillus cereus* strain ROC. *PloS one*, 17(6), e0269559. [10.1371/journal.pone.0269559](https://doi.org/10.1371/journal.pone.0269559)
43. Lalnunhlimi S., Krishnaswamy V. 2016. Decolorization of azo dyes (Direct Blue 151 and Direct Red 31) by moderately alkaliphilic bacterial consortium. *Brazilian Journal of Microbiology*, 47(1), 39-46. <https://doi.org/10.1016/j.bjm.2015.11.013>